

Two-dimensional diffraction of plasma, thermal, and elastic waves generated by an infrared laser pulse in semiconductors

B. Audoin, H. Meri, and C. Rossignol

Laboratoire de Mécanique Physique, UMR CNRS, no. 5469, Université Bordeaux I, 33405 Talence, France

(Received 29 September 2006; revised manuscript received 20 October 2006; published 26 December 2006)

When a 1064 nm laser pulse is focused at the surface of silicon, it has been observed that the material contracts whereas heating should produce expansion. In addition to the usual thermal acoustic source, a nonthermal sound generation results of photoexcitation of electron-hole pairs. To describe the optoacoustic effect in semiconductors, it is thus necessary to account for thermoelastic and other deformation sources simultaneously. The acoustic signal is then strongly dependent on the nature of the space-time evolution of both the photoexcited charge carriers and temperature. In this paper, assuming line focusing of the laser pulses, a model is implemented that accounts for the two-dimensional (2D) character of charge carrier motion and heat conduction. Relevant differential equations are coupled together and with the wave motion equation to describe acoustic diffraction. Three sets of equations are linearized in a 2D Fourier domain and solutions are found with an appeal to convenient boundary conditions. The conditions for 2D diffraction of plasma, thermal, and elastic waves are analyzed. Experiments are performed on a 5 mm thick silicon plate with a Nd:yttrium aluminum garnet laser that delivers 20 ns pulses. Signals are measured for epicenter and off epicenter positions. Very good agreement is obtained with calculated signals for both positions demonstrating that both sound generation mechanism and anisotropy are accurately taken into account. In addition to the expected material contraction accompanying quasilongitudinal bulk acoustic waves, the other remarkable feature is the change in the shape of the signals observed for a same angle, but for two laser energies. The results emphasize the nonlinear photoacoustic response of the material, with respect to the laser energy. It is accurately represented by the calculations, assuming prevailing of Auger electron-hole recombination process and nonlinear dependency of charge carrier lifetime with respect to its density.

DOI: [10.1103/PhysRevB.74.214304](https://doi.org/10.1103/PhysRevB.74.214304)

PACS number(s): 43.35.+d

I. INTRODUCTION

The volume contraction of a silicon crystal under intense illumination by laser light has been the motivation to study the ultrasound generation by the concentration-deformation mechanism in semiconductors.¹ It was shown that the lattice contraction can be interpreted in terms of the semiconductor crystal's volume dependence on the occupation of the electronic energy levels. The density of excess electrons in the conduction band, thus of holes in the valence band, is connected with the derivative of the band-gap energy with respect to pressure. The contraction effect comes from the negative sign of the derivative for silicon. These phenomena have been deeply studied, but to our knowledge, the anisotropic diffraction of the so-generated acoustic waves, and its connection with charge carriers and temperature diffusion, has never been analyzed. To this purpose, the space and time evolution of laser-induced plasma in semiconductors, together with its link to temperature rise, must be correctly accounted for.

The physical processes that occur during and after light absorption by semiconductors have been extensively studied.²⁻⁵ These processes start with the direct absorption of a photon from the incident pulse by an electron which makes a transition from the valence to the conduction band. Such a transition is allowed when the energy of the photon is greater than the direct band gap. Free carriers absorption is the process in which an electron once in the conduction band makes a transition to a state higher in that band by means of the simultaneous absorption of a photon and the emission of a

phonon. An identical process occurs for holes in the conduction band. Electrons located high in the conduction band may relax within that band by phonon emission. The effect of this relaxation is to reduce the electron temperature and increase the lattice temperature. Neither free carrier absorption nor electron relaxation changes the number of free carriers. At the reverse, recombination processes, either radiative or non-radiative, reduce the number of charge carriers. The nonradiative recombination in which a plasmon is emitted does not prevail at the large time scale considered in this paper. The radiative recombination of an electron in the conduction band with a hole in the valence band by means of the simultaneous emission of a photon and of a phonon is important. The subsequent dynamics of the dense electron-hole plasma was extensively explored.⁶ The carriers' ambipolar diffusion was also studied to determine the extent of the heated zone, which can be much larger than the array in which light penetrates.⁷ For pulses of ns time duration, a model was developed to describe the kinetic of the laser-induced plasma in germanium and silicon. It takes into account the processes mentioned above, and also the carrier concentration and the temperature gradient.⁸ For light pulses in the ps range, van Driel⁹ proposed equations to describe the kinetic of dense plasma. Using coupled equations, the carrier density and the temperature were calculated. In addition, Auger recombination process, occurring when a high density of free carriers is generated, was analyzed with modulated photoreflectance.¹⁰ In this context, the free carrier lifetime is no longer considered as a constant, but it is proportional instead to the inverse of the square of charge density.¹¹

The absorption of light by a semiconductor provokes the increase of carrier density and also the rising of both the lattice and carrier temperatures. In situations where ns laser pulses with high power density interact with the semiconductor, it is generally acknowledged that the carrier and lattice temperatures are essentially the same.¹² However, Lietoila and Gibbons¹³ have proposed a calculation of these three quantities for ns laser pulses. They have shown that free carrier absorption plays a major role with 1.06 μm radiation and that Auger recombination coefficient is not sensitive to temperature.

In most materials, the photoacoustic generation results from photothermal and thermoacoustic mechanisms. The heating of a volume of the material and subsequent dilatation acts as an acoustic source. The acoustic strain may in turn yield heating that is generally neglected. Temperature diffusion equation and acoustic wave equation are thus partly coupled. However, in semiconductors, the changes in carrier density involve strain. The so-called electron-deformation mechanism can thus act as an additional acoustic source. The generated acoustic strain may in turn generate plasma waves, acting as a thermal source itself. Thus electronic, thermal, and acoustic waves are coupled. Their couplings have been under the scope of several studies. Stearns and Kino¹⁴ have proposed a partial coupling between the electronic, thermal, and acoustic phenomena. In their unidimensional modeling, the recombination mechanism is not considered in the carrier diffusion equation, and neither is the coupling with temperature and strain. The temperature diffusion equation is also considered without taking into account the acoustic source. They have shown from both theoretical and experimental results that the electron-deformation mechanism may dominate in the photoacoustic response. Another more complete unidimensional modeling, still including partial coupling, was proposed by Akhmanov and Gusev¹⁵ and Gusev and Karabutov.¹⁶ They have considered a linear carrier diffusion equation including nonradiative recombination, ambipolar diffusion, and optic absorption, without coupling effect with temperature and strain. However, coupling with the nonradiative recombination is included in the temperature diffusion equation in addition to the thermal source resulting of the absorption of light. Stress associated with electron-deformation is introduced as a source term in the acoustic equation together with the thermal stress. The important effect of Auger recombination was pointed out. They have also performed a complete frequency analysis allowing one to identify the dominating terms in these equations at different time scales. It was shown that the electron-deformation process may dominate the acoustic response also when fs pulses are used. For such short pulses, the dynamics of both bulk and surface recombination mechanisms, and of temperature and carrier diffusion, can be neglected with respect of ultrafast acoustic response.¹⁷ When subnanosecond pulses are considered, it was demonstrated that the coupling between plasma and acoustic waves may yield broadening of the acoustic pulses.¹⁸ In addition, Todorovic *et al.*^{19–21} have proposed a quantitative analysis of the coupling effects and they have analyzed the conditions in which the complete coupling between carrier, temperature, and acoustic equations can be neglected. Recently, Dixon *et al.*²² have illustrated experi-

mentally the changes in the shape of the longitudinal acoustic signal with the fluence of the laser pulses in silicon. Whereas a negative pulse corresponding to contraction is measured at low intensity, dilatation yields positive pulses for higher intensities, and bipolar signals are measured in the intermediate regime.

In this paper, a two-dimensional (2D) model for the photoacoustic transduction in anisotropic semiconductors is considered to calculate the acoustic waves diffracted in the material when the laser beam is focused on its surface. The theoretical results mentioned above have allowed introducing 2D linear wave equations for carrier density, temperature, and acoustic displacement vectors. These partly coupled equations and their solving are presented in Sec. II together with the boundary equations. In Sec. III, the conditions in which 2D diffraction of plasma, thermal, and acoustic waves occurs are discussed on the basis of analytic results derived in the frequency-wave number domain. Then, in Sec. IV, experimental and calculated results obtained for ns pulses and for various laser intensities show the influence of Auger recombination time on the polarity and shape of both the quasilongitudinal and quasishear diffracted acoustic waves.

II. 2D WAVE EQUATIONS FOR SEMICONDUCTORS

A homogeneous semiconducting material is considered. The material elasticity, thermal conductivity, and charge carrier diffusivity are assumed to show orthotropic symmetry in the same (x_1, x_2, x_3) axes. The sample is a parallel-sided plate of thickness h and it is cut such that axis x_1 lies along the normal to the plate.

The optical axis of the incident laser radiation is x_1 , and the incident light is focused at the surface $x_1=0$ along a line in the direction x_3 . Neglecting the laser beam expansion due to focusing or to optic dispersion, the volume and time density of the energy brought by the incident light inside the medium is given by

$$Q(x_1, x_2, t) = \beta I(1 - R)g(x_2)f(t)e^{-\beta x_1}, \quad (1)$$

where I is the incident energy by unit of length, R denotes the optical reflectivity, and β stands for the optical absorption coefficient. For semiconductors under laser illumination, it has been observed that the reflectivity increases with light intensity, and so does the optical absorption. However, this effect is not considered in this paper, assuming that the optical penetration does not depend on plasma density, or on temperature. This assumption allows one to consider that the optical absorption remains uniform along the sample surface also. In Eq. (1), $g(x_2)$ and $f(t)$ represent the normalized space and time distributions of the line source radiation, respectively.

In the following, the energy E of each incident photon is supposed to be greater than the semiconductor energy band-gap E_g . Therefore electrons are extracted from the valence band of the crystal to the conduction band, and electron-hole pairs are generated. The equations used to describe their diffusion are now presented.

A. Plasma wave equation

The dynamics of electrons and holes are not dissociated in this paper. The time and space dependency of the plasma density N is governed by the 2D electron diffusion and by the nonradiative electron-hole recombination. Assuming Auger recombination is the dominant recombination mechanism, the corresponding diffusion equation is⁷

$$\frac{\partial N}{\partial t} - \nabla \cdot (\Lambda \nabla N) + \frac{1}{\tau_R} N = \frac{Q(x_1, x_2, t)}{E}. \quad (2)$$

Here Λ stands for the ambipolar (carrier) diffusion tensor. Since this equation has been essentially used up to now for only one-dimensional (1D) plasma diffusion, an appeal to this second-order tensor instead of the usual ambipolar diffusion coefficient is not common. In Eq. (2), the nonradiative Auger recombination is taken into account by the third term in the left-hand side. There, τ_R represents the lifetime of charge carriers, the so-called Auger recombination time. Since lifetime depends on the recombination probability, it is inversely proportional to the square of charge density, $\tau_R \propto N^{-2}$.^{23,24} This gives to Eq. (2) a nonlinear nature. However, a characteristic value of N , not depending on space and time but proportional to the incident light intensity, can provide a good estimate for τ_R .¹⁶ The right-hand side of Eq. (2) describes the photogeneration of charge carriers; it expresses that each photon creates one electron-hole pair. One should notice that the interaction of temperature or phonons with charge carrier density is neglected in Eq. (2).

Let us now pay attention to the boundary condition for the plasma field. Since recombination is enhanced at the air-material interface, lifetime of charge carriers at the surface is smaller than in the bulk of the semiconductor material. Consequently, charge carrier density is smaller at the surface, giving rise to diffusion from the bulk of the material toward its surface. Therefore, the boundary condition expressing that the charge flux through the surface is null, i.e., that the surface recombination at high speed S is balanced by the subsequent bulk to surface diffusion, is¹²

$$\left(\Lambda_{11} \frac{\partial N}{\partial x_1} - SN \right)_{x_1=0} = 0. \quad (3)$$

Assuming that the optical penetration depth, as well as the diffusion length during characteristic times, is small with respect to the sample thickness, it is not necessary to take into account the boundary condition at the rear surface $x_1=h$.

At this point, interest is turned to the thermal field, which strongly depends on the time and space evolution of the plasma density.

B. Thermal wave equation

At ns time scale, it is generally acknowledged that the lattice and carrier temperatures are equal.¹² The temperature field $T(x_1, x_2, t)$ inside the material results of both optothermal and optoelectronic effects. It satisfies the following diffusion equation:

$$\rho C_p \frac{\partial T}{\partial t} - \nabla \cdot (\boldsymbol{\kappa} \nabla T) = (E - E_g) \frac{Q(x_1, x_2, t)}{E} + \frac{E_g}{\tau_R} N, \quad (4)$$

where ρ stands for the mass density, C_p denotes the specific heat, and $\boldsymbol{\kappa}$ is the thermal conductivity tensor.

As already mentioned, each photon brings one electron from the valence band to the conduction band. It immediately falls down to the minimum of the conduction band. The energy released for thermalization is then $E - E_g$. Therefore, the first term in the right-hand side of Eq. (4) quantifies the amount of the incident energy that is directly thermalized. The last term describes crystal heating from the energy released by the charge carriers that recombine during Auger time.

The left-hand side of Eq. (4) is similar to that of the classical parabolic Fourier diffusion equation, assuming that the temperature rise follows instantaneously the source rise. Since the characteristic rise time is of the order of ps for most metals and semiconductors, this assumption is valid for these materials when the thickness is of the order of millimeter. For thinner samples, the hyperbolic diffusion equation in either of its form should be preferred.²⁵

The heat boundary equation is now considered, assuming adiabatic conditions at the surface. Owing to the high recombination rate at the surface, electrons release energy for thermalization, so generating heat flux at the surface. Taking also into account heat flux resulting from temperature diffusion, one gets the following boundary equation:

$$\left(\kappa_{11} \frac{\partial T}{\partial x_1} + E_g SN \right)_{x_1=0} = 0. \quad (5)$$

As for the diffusion of charge carriers, it is assumed here that the temperature diffusion length during characteristic times is small with respect to the sample thickness. Therefore, the boundary condition at the rear surface $x_1=h$ is not considered.

Once basic equations describing the 2D diffusion of charge carriers and temperature are stated, one can investigate the acoustic wave propagation equation in semiconducting materials.

C. Acoustic wave equation

The acoustic wave equation accounting for thermoelastic and electronic deformation mechanisms, is written as

$$\rho \frac{\partial^2 \mathbf{u}}{\partial t^2} - \nabla \cdot (\mathbf{C} : \nabla_s \mathbf{u}) = -\lambda \nabla T - \mathbf{D} \nabla N, \quad (6)$$

where \mathbf{u} stands for the displacement vector at any position and time, and \mathbf{C} denotes the fourth order stiffness tensor. $\lambda = \mathbf{C} : \boldsymbol{\alpha}$ is the thermal rigidity tensor in which $\boldsymbol{\alpha}$ is the thermal expansion tensor of the material. The coupling between plasma density and stress is introduced by mean of the tensor of electroacoustic coupling $\mathbf{D} = \mathbf{C} : \mathbf{d}$,¹⁴ accounting for the difference in deformation potential of the conduction and valence bands. The parameter \mathbf{d} quantifies the changes with stress of the band gap energy E_g . Instead of the scalar expression that was used up to now with the scalar wave propa-

gation equation,¹⁶ we introduce the following components for tensor \mathbf{d} :

$$d_{ij} = -\frac{\partial E_g}{\partial \sigma_{ij}}, \quad i, j = 1 \dots 3, \quad (7)$$

where σ_{ij} are components of the stress tensor.

Boundary conditions for the displacement field must also be stated since they are derived to obtain analytic and numerical results discussed in the following sections. Since light is focused along a line lying along a principal direction of the material symmetry, free loaded conditions lead to null values of stiffness components σ_{11} and σ_{12} only. Moreover, owing to negligible acoustic attenuation in crystals at the considered ultrasonic frequencies, waves reflected at the interfaces may propagate forth and back through the plate. The two interfaces are thus considered in the following boundary equations:

$$\left(C_{11} \frac{\partial u_1}{\partial x_1} + C_{12} \frac{\partial u_2}{\partial x_2} - \lambda_1 T - D_1 N \right)_{x_1=0,h} = 0, \quad (8)$$

$$C_{66} \left(\frac{\partial u_1}{\partial x_2} + \frac{\partial u_2}{\partial x_1} \right)_{x_1=0,h} = 0.$$

In these equations and in the following, the abbreviated subscript notations are used for components of tensors \mathbf{C} , λ , and \mathbf{D} .

D. Calculations of 2D plasma, thermal, and acoustic fields

As mentioned in Sec. II A, the plasma wave equation is a nonlinear equation of N . However, this feature vanishes when the Auger combination time is approximated to a constant value that depends on the incident light intensity. With this assumption, the 2D plasma, thermal, and acoustic fields can be calculated using Fourier transformations on space, x_2 , and time variables. Let k_2 and ω denote the Fourier dual variables, respectively. Applying these transforms yields a set of linear partial derivative equations with respect to the depth x_1 only. The solution is composed of a sum of exponential functions of x_1 . For a fixed (k_2, ω) , solving dispersion equations associated with propagation Eqs. (2), (4), and (6) provides components $j\Pi$, $j\Gamma$, and k_1 , along x_1 , of plasma, thermal, and acoustic waves vectors, respectively. The amplitudes are obtained with an appeal again to propagation Eqs. (2), (4), and (6), and also with the help of boundary Eqs. (3), (5), and (8).

The displacement \mathbf{u} at a given position x_2 and time is calculated in the sequel by numerical inversions of the spatiotemporal Fourier transformations of the solution $\tilde{\mathbf{u}}$ calculated in the (k_2, ω) Fourier space. Note that the temperature $T(x_2, t)$ and plasma density $N(x_2, t)$ would also have been mapped using the same calculation scheme. Moreover, acoustic displacement can be calculated on either side $x_1 = \pm h/2$ of the plate.

The above calculations were presented for a line source along a principal direction for the purpose of clarity. However, a line source along any direction could be considered as

well. Moreover, when the anisotropic material symmetry is limited to axisymmetries with respect to axis x_1 , a point source can be considered in the modeling without bringing additional numerical burden, so long as the space Fourier transform is changed in a Hankel transform.

In the next section, interest is focused on some analytic expressions obtained in the Fourier domain for the three fields of interest: $\tilde{N}(k_2, \omega)$, $\tilde{T}(k_2, \omega)$, and $\tilde{\mathbf{u}}(k_2, \omega)$.

III. SPECTRAL ANALYSIS FOR SILICON

A spectral analysis of the prevalence of the physical phenomena involved in the plasma and temperature waves generation and diffusion has been under the scope of several previous papers.^{15,16} Further analysis is brought in this section to state the conditions on the incident laser intensity, the source size, and the frequency ranges for which the plasma or thermal field are diffracted in two dimensions by the optic source.

In the context of the assumptions mentioned in Sec. II, the expressions detailed in the followings are general for semiconductors. However, since quantitative discussions will now be based on numerical applications for silicon, let us draw the main features of the considered sample.

A. Silicon sample

The cut of the silicon plate is such that its normal, axis x_1 , lies along the crystallographic direction $[1,1,0]$. Directions x_2 and x_3 belonging to the sample surface, correspond to crystallographic axes $[-1,1,0]$ and $[0,0,1]$, respectively. Since silicon crystal exhibits a cubic symmetry, axes x_1 and x_2 are principal axes. Accordingly, with the sample axes, the material shows a tetragonal symmetry and its stiffness coefficients can be calculated from reference values for silicon. On using contracted subscripts convention, the stiffness coefficients are such that the stiffness tensor can be written in the following matrix form:

$$\mathbf{C} = \begin{pmatrix} 194.36 & 35.24 & 63.90 & & & \\ & 194.36 & 63.90 & & & 0 \\ & & 165.70 & & & \\ & & & 79.56 & & \\ & \text{sym.} & & & 79.56 & \\ & & & & & 50.90 \end{pmatrix} \quad (9)$$

in GPa.

The material mass density is $\rho = 2.332 \text{ g cm}^{-3}$, and the plate thickness is $h = 5 \text{ mm}$. The anisotropy of acoustic waves velocity is mapped in Fig. 1 where the group velocities of quasilongitudinal (L) and quasishear (T) waves are plotted in the plane (x_1, x_2) . High anisotropy leads to the characteristic shape of the quasishear mode, which contains cuspidal edges where the curve folds back on itself. A third acoustic mode with polarization along the x_3 direction may propagate. It is not shown in Fig. 1 since this mode is not generated when a line source is oriented along the axis x_3 .

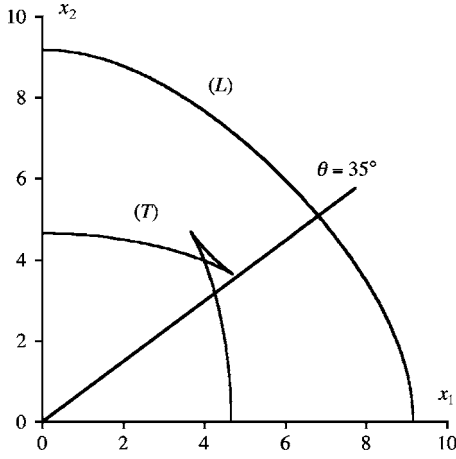


FIG. 1. Group velocity curves (km/s) in the plane (x_1, x_2) of the silicon sample.

Let us now accurately state the optic, electronic, and thermal properties considered in the remainder. Note that owing to the cubic symmetry of silicon the ambipolar diffusion, thermal expansion, and thermal conductivity tensors, which are of order 2, have a spherical form in the crystal axes, and in the sample axes as well. The material optic properties are $R=0.33$ and $\beta=1.4 \text{ mm}^{-1}$ at a laser wavelength of 1064 nm; the material thermal coefficients are $C_p=757 \text{ J K}^{-1} \text{ K}^{-1}$, $\alpha_i=1.2 \times 10^{-5} \text{ K}^{-1}$, and $\kappa_i=150 \text{ Wm}^{-1} \text{ K}^{-1}$, $i=1 \dots 6$; and the scalar electronic parameters are $E_g=1.12 \text{ eV}$, and $S=10^2 \text{ ms}^{-1}$. Let's remark that great dispersion exists in the values found in the literature for the surface electron-hole recombination velocity S , ranging from 10 ms^{-1} to 10^4 ms^{-1} , since this parameter is highly sensitive to the surface roughness. The electronic tensor components are $\Lambda_i=35 \times 10^{-4} \text{ m}^2 \text{ s}^{-1}$, and $d_i=-9.5 \times 10^{-24} \text{ cm}^3$, $i=1 \dots 6$. The latter components are the scalar values used in the literature to describe 1D charge carriers diffusion in silicon.^{14,16} The negative sign of d_i is a characteristic feature of electroacoustic effects in silicon. As a consequence, components of tensors λ and D have opposite signs, and the acoustic sources in the right-hand side of Eq. (6) have opposite effects: cold plasma acoustic generation yields material contraction, whereas temperature rise generates expansion.

Once the material properties have been stated, the conditions for 2D diffraction of plasma and temperature fields are discussed quantitatively in the following paragraphs.

B. Spectral analysis of plasma field

Solving the plasma wave equation as described in Sec. II yields the following explicit form for the charge carriers field \tilde{N} in the (k_2, ω) domain:

$$\tilde{N} = \frac{\tilde{Q}}{E\Lambda_1(\Pi^2 - \beta^2)} \left(e^{-\beta x_1} - \frac{\Lambda_1\beta + S}{\Lambda_1\Pi + S} e^{-\Pi x_1} \right). \quad (10)$$

In this equation,

$$\tilde{Q} = \beta I (1 - R) \tilde{g}(k_2) \tilde{f}(\omega), \quad (11)$$

where $\tilde{g}(k_2)$ and $\tilde{f}(\omega)$ stand for the Fourier transforms of the space and time distribution of the line source radiation, respectively; and Π is such that

$$\Pi^2 = \frac{1}{\Lambda_1} \left(\Lambda_2 k_2^2 + \frac{1}{\tau_R} + j\omega \right). \quad (12)$$

The 2D character is driven by the latter equation. Diffraction has to be considered (i) when τ_R^{-1} is negligible with respect to $\Lambda_2 k_2^2$, or of the same order as $\Lambda_2 k_2^2$: $\tau_R^{-1} \leq \Lambda_2 k_2^2$; and (ii) for frequencies such that $\omega \leq \Lambda_2 k_2^2 + \tau_R^{-1}$. Since the Auger recombination time τ_R is correlated to the incident laser intensity, it should be noticed at this stage that the 2D character of carrier diffusion depends not only on the frequency but also on the light intensity.

On noting that $k_2 < 2/a$, where a denotes the width at midheight of the source, condition (i) can be rewritten as $\sqrt{\Lambda_2} \tau_R \geq a/2$, expressing that the plasma diffusion length in direction x_2 during Auger time must be greater, or of the same order, than half the source aperture. In other words, writing condition (i) as $\tau_R \geq a^2/4\Lambda_2$, it appears that the Auger recombination time must be greater, or of the same order as the time for plasma to diffuse in direction x_2 at a distance equal to half the source width. Focusing the incident laser beam to an extremely small width $a=1 \text{ }\mu\text{m}$, one gets diffusion time of the order of 71 ps. Auger recombination time is greater for laser intensities currently used for most experiments. The limit value turns to $0.71 \text{ }\mu\text{s}$ when the laser beam is focused to an easily achievable spot size of 0.1 mm. As illustrated later in Sec. IV, Auger time can be on either side of this limit, depending on light intensity. Let us underline that condition (i) does not depend explicitly on frequency and that directivity of the plasma field can be driven by light intensity.

When the later condition on Auger time is provided, condition (ii) yields a relationship that is currently encountered in diffusive phenomena. It relates the spot size and the frequencies, $\omega \leq 4\Lambda_2/a^2$. This condition is achieved for frequencies up to 1.4 MHz for silicon when the spot size is about 0.1 mm.

C. Spectral analysis of temperature field

Solving the thermal wave equation as described in Sec. II with the expression for \tilde{N} given in Eq. (10) yields the following explicit form for the temperature field \tilde{T} in the (k_2, ω) domain:

$$\tilde{T} = A_T e^{-\beta x_1} + B_T e^{-\Pi x_1} - \frac{1}{\Gamma} (\beta A_T + \Pi B_T) e^{-\Gamma x_1}. \quad (13)$$

In this equation,

$$A_T = \frac{\tilde{Q}}{\rho C_p \chi_1 (\Gamma^2 - \beta^2)} \left[\frac{E - E_g}{E} - \frac{E_g}{E\Lambda_1 \tau_R (\Pi^2 - \beta^2)} \right],$$

$$B_T = - \frac{E_g}{\tau_R \rho C_p \chi_1 (\Gamma^2 - \Pi^2)} \frac{\tilde{Q}}{E\Lambda_1 (\Pi^2 - \beta^2)} \frac{1}{(\Lambda_1 \Pi + S)}, \quad (14)$$

and Γ is such that

$$\Gamma^2 = \frac{1}{\chi_1}(\chi_2 k_2^2 + j\omega) \quad (15)$$

on noting $\chi_i = \kappa_i / \rho C_p$, $i = 1, 2$.

The 2D character of the temperature is driven by the conditions discussed above for Π , and by the following for Γ : $\omega \leq \chi_2 k_2^2$, which is general for 2D thermal diffusion. It expresses that the source size must be small with respect to the distance the temperature diffuses in the direction x_2 during characteristic times ω^{-1} . This condition is satisfied for frequencies below 0.34 MHz for a spot size around 0.1 mm. If the laser intensity is such that condition (i) on τ_R is satisfied, then for frequencies between 0.34 MHz and 1.4 MHz the 2D character of the temperature field comes only from the 2D diffusion of electrons during Auger recombination time. The existence of such a bandwidth can be generalized to other semiconducting materials since for most of them Λ_2 is greater than χ_2 , and these two parameters are in general in a ratio of about 100.

D. Lateral extent of the acoustic source

The 2D expansion of the plasma and temperature fields obviously influences the shape of the photoacoustic source and the quantitative description is not straightforward. However, a rough limit condition for the diffraction of quasilon- gitudinal and quasishear acoustic waves is that the lateral extent a_A of the acoustic source be such that $k_{2T} a_A < 1$, where k_{2T} denotes the wave number of the quasishear mode along the interface. Since carrier diffusion is a faster phenomena than temperature diffusion, the lateral extent of the source can be approximated with the diffusion length of plasma along the interface, $a_A = \sqrt{\Lambda_2 \tau_R}$. For acoustic frequencies in the MHz range, the rough condition requires that τ_R be smaller than 0.1 ms for silicon, which is far satisfied in our experiments.

IV. CALCULATION AND EXPERIMENTAL RESULTS

A. Experimental setup

Let us briefly describe the experimental setup. A Nd:YAG (yttrium aluminum garnet) laser is used to provide photons with an energy of 1.17 eV, above the indirect band gap $E_g = 1.11$ eV of silicon at room temperature. At this wavelength, a large portion of the absorbed energy may be expected to produce electron-hole pairs. The laser delivers pulses of about 20 ns in duration, and the maximum output energy is about 300 mJ per pulse. The laser beam is focused on the front surface, $x_1 = -h/2$, of the semiconducting sample. A convenient set of lenses is used to form a line illumination. The length and width of the line are about 2 cm and 0.1 mm, respectively. By making use of a system composed of moveable mirrors, the setup allows the displacement of the source along the surface in a direction normal to the line.

A doubled Nd:YAG laser at 532 nm is used in a laser interferometer,²⁶ which is focused into a point at the rear surface of the sample, $x_1 = h/2$. It measures the normal surface displacements, allowing one to detect the acoustic wave

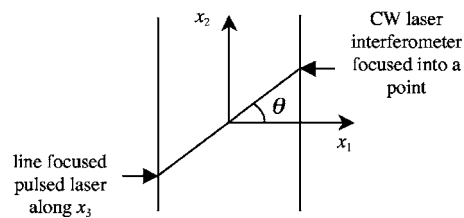


FIG. 2. Pulsed and CW lasers location with respect to the sample geometry.

arrivals. As shown in Fig. 2, the angle θ between axis x_1 and the source to detector direction defines the observation angle of the 2D waves diffraction, with respect to the plate normal. Signals are downloaded from a digital oscilloscope into a computer, where they are stored for postprocessing.

B. Calculated and experimental signals

The component normal to the interface of the acoustic displacement was measured for several source-receiver directions θ and for several laser intensities I . The wave forms recorded for the epicenter position $\theta = 0$ and a nonepicenter position $\theta = 35^\circ$, and for two laser intensities I_1 and I_2 are shown in Fig. 3. The signals calculated for the same two angles are also displayed in Fig. 3. The only calculation parameter that was tuned to fit experimental data was the incident laser intensity. Values of $I_1 = 7.5 \text{ mJ m}^{-1}$ and $I_2 = 200 \text{ mJ m}^{-1}$ were so identified. They are in agreement with the ability of the experimental device. The corresponding Auger recombination times, calculated¹⁶ with the Auger constant for silicon $\gamma = 4 \times 10^{-31} \text{ cm}^6 \text{ s}^{-1}$ are $\tau_{R1} = 17 \text{ }\mu\text{s}$ and $\tau_{R2} = 24 \text{ ns}$, respectively. Very good agreement between the calculated and experimentally recorded signals was obtained for intensity I_1 , Figs. 3(a) and 3(b). Agreement is also good for the highest intensity I_2 , Figs. 3(c) and 3(d), despite slight experimental artifacts that may be due to surface burning. Comparison of the wave forms allows us to bring the comments detailed in the following section.

C. Result analysis

The first remarkable feature emphasized in Fig. 3 is that the acoustic displacement associated to the first longitudinal wave arrival has a negative amplitude for both laser energies I_1 and I_2 , i.e., the surface firstly moves towards the bulk of the sample. At the reverse, signals calculated for a very high energy, not plotted in Fig. 3, are opposite in shape to the signals shown in Figs. 3(a) and 3(b). However, such wave forms cannot be experimentally recorded since the relevant energy is higher than the surface ablation threshold for silicon, and the actual process would be neither electronic nor thermal but it results from the ejection of a gas plasma generated by the melting of the sample surface. The material contraction observed in Fig. 3 underlines that for these weak laser energies the electronic volume effect dominates the thermoacoustic generation.

The second remarkable point is the change in the shape of the signals observed for a same angle, but for two laser energies. This change emphasizes the nonlinear response of the

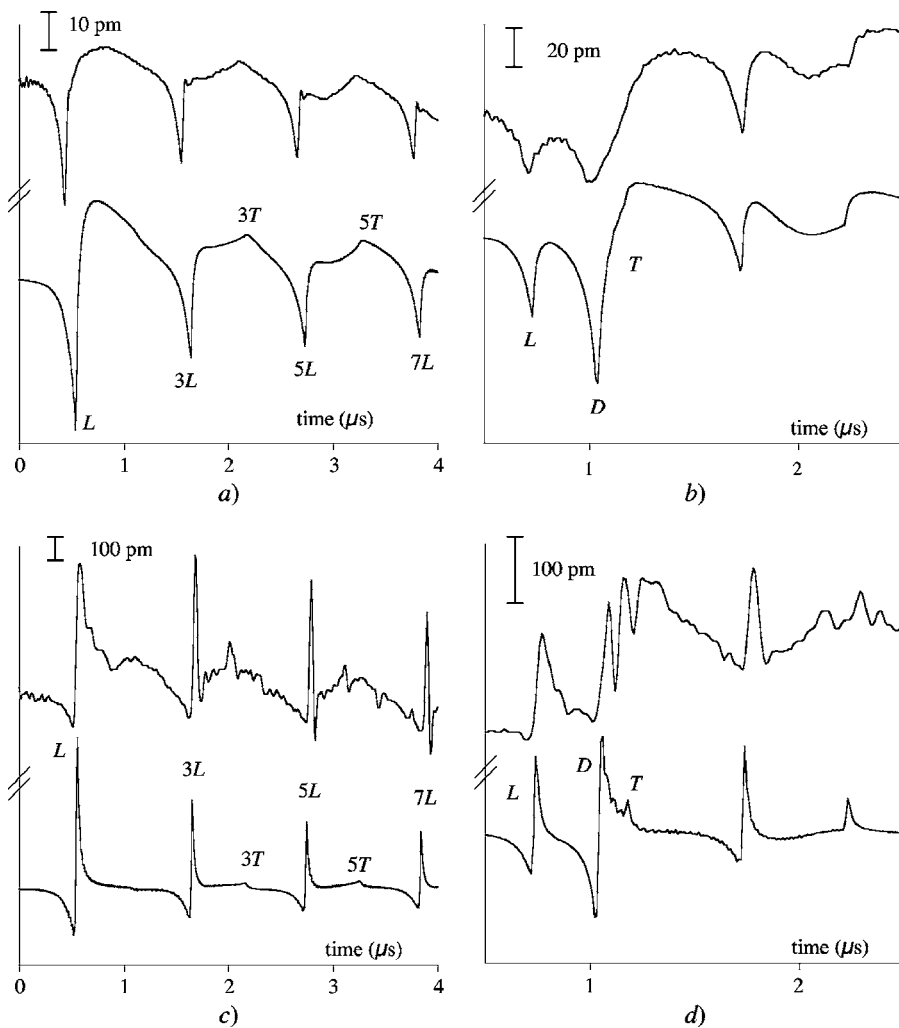


FIG. 3. Experimental (up) and calculated (down) signals in silicon for two source-receiver directions: $\theta=0^\circ$ (a) and (c) and $\theta=35^\circ$ (b) and (d); and two incident laser energies: $I_1=7.5 \text{ mJ m}^{-1}$ (a) and (b) and $I_2=200 \text{ mJ m}^{-1}$ (c) and (d).

material, with respect to the laser energy. It is in agreement with the predictions also provided in Refs. 15 and 16 for plane longitudinal and Rayleigh acoustic waves. The change comes from the nonlinear dependency of the Auger recombination time with respect to laser energy. For very weak laser energies, τ_{R_1} is extremely large compared to the time scale in Fig. 3. Therefore, the time evolution of the electroacoustic source is approximately a Heaviside step function. At the reverse, for a larger energy, the lifetime τ_{R_2} of the photoexcited electron-holes is so small that the electroacoustic source can be assimilated to a delta function in time. As a consequence, the shape of the wave forms in Figs. 3(a) and 3(b) is the time derivative of that in Figs. 3(c) and 3(d), respectively.

Owing to the small lateral size of the acoustic source, both longitudinal and shear waves are diffracted by the source. Moreover, as another result of diffraction, the waves associated with shear modes have a nonzero component in the direction normal to the film surface and thus, their normal amplitude can be measured by laser interferometry even at the epicenter position, as shown in Figs. 3(a) and 3(c). Successive echoes of waves propagating back and forth through the plate provide observations of the acoustic field at increasing travel distances from the source. From the near field to the far field, amplitude of the shear wave increases.²⁷

For a source width of approximately 0.1 mm and an Auger time of $\tau_{R_1}=17 \mu\text{s}$, the condition $\tau_R \geq a^2/4\Lambda_2$, Sec. III B, is verified and 2D diffraction of plasma field occurs. At the reverse, this relation is not satisfied for $\tau_{R_2}=24 \text{ ns}$. As a consequence, the amplitude of the shear waves 3T, 5T are slightly weaker, with respect to their longitudinal counterparts 3L, 5L, in Fig. 3(c) than in Fig. 3(a).

Large waves denoted D in Figs. 3(b) and 3(d) appear between the quasilongitudinal L and quasishear wave T for an observation angle of $\theta=35^\circ$. However, only two waves should be observed for this direction according to the energy radiation diagram shown in Fig. 1, since it does not belong to the cusp sector. This third acoustic wave arrival is not predicted by ray theory. In order to explain the existence of such wave, the finite wavelength of the acoustic waves must be considered. Indeed, diffraction occurs at the extremities of the cusp, and ultrasounds are detected in directions for which no acoustic ray can be calculated. Maris has described this diffraction phenomenon in the geometrical shadow, extrapolating for the study of phonon focusing²⁸ the works of Pearcey performed in electromagnetism.²⁹ The phenomenon was also experimentally observed at ultrasonic frequencies using focused monochromatic acoustic sources.³⁰ Its observation when a broadband laser source is used, and its effect on materials characterization, was discussed in Ref. 31. This

wave D is the signature of the diffraction of the quasishear mode propagating in an anisotropic medium. Waves T and D in Figs. 3(b) and 3(d) provide great evidence of the acoustic diffraction of the waves generated by the cold plasma electroacoustic process.

V. CONCLUSIONS

A model that takes into account simultaneously the generation and diffusion of dense electron-hole plasma and of thermal field in semiconductors was developed to represent the anisotropic scattering of the so-generated acoustic waves. It was successfully applied to represent the wave forms generated with ns laser pulses in a 5 mm thick silicon crystal. The nonlinear response of the material with respect to the

incident light intensity was demonstrated for epicenter and nonepicenter measurement positions. For incident intensity less than the ablation threshold, the electron deformation generation mechanism prevails on the thermoacoustic process. Measurement and modeling of the acoustic diffraction of both quasilongitudinal and quasishear waves generated by the cold plasma electroacoustic process is an unprecedented result. It opens opportunities for the nondestructive evaluation of electron-hole diffusion parameters in semiconductors.

Work underway is focused on the propagation of acoustic waves generated with ultrashort laser pulses in micrometer thick semiconductors. Correct understanding of the propagation of the so-generated acoustic waves in such materials is of great importance for the application of picosecond ultrasonics to the nondestructive control and evaluation of assembly in the microelectronic industry.

-
- ¹W. B. Gauster and D. H. Habing, Phys. Rev. Lett. **18**, 1058 (1967).
²A. Elci, M. O. Scully, A. L. Smirl, and J. C. Matter, Phys. Rev. B **16**, 191 (1977).
³H. M. van Driel, Phys. Rev. B **19**, 5928 (1979).
⁴D. von der Linde and R. Lambrich, Phys. Rev. Lett. **42**, 1090 (1979).
⁵C. V. Shank, R. L. Fork, R. F. Leheny, and J. Shah, Phys. Rev. Lett. **42**, 112 (1979).
⁶E. J. Yoffa, Phys. Rev. B **21**, 2415 (1980).
⁷J. F. Young and H. M. van Driel, Phys. Rev. B **26**, 2147 (1982).
⁸J. S. Preston and H. M. van Driel, Phys. Rev. B **30**, 1950 (1984).
⁹H. M. van Driel, Phys. Rev. B **35**, 8166 (1987).
¹⁰B. C. Forget, D. Fournier, and V. E. Gusev, Appl. Phys. Lett. **61**, 2341 (1992).
¹¹A. Haug, Solid-State Electron. **21**, 1281 (1978).
¹²M. I. Gallant and H. M. van Driel, Phys. Rev. B **26**, 2133 (1982).
¹³A. Lietoila and J. F. Gibbons, J. Appl. Phys. **53**, 3207 (1982).
¹⁴R. G. Stearns and G. S. Kino, Appl. Phys. Lett. **47**, 1048 (1985).
¹⁵S. A. Akhmanov and V. E. Gusev, Sov. Phys. Usp. **35**, 153 (1992).
¹⁶V. E. Gusev and A. A. Karabutov, *Laser Optoacoustics* (AIP Press, New York, 1993).
¹⁷O. B. Wright and V. E. Gusev, Appl. Phys. Lett. **66**, 1190 (1995).
¹⁸N. V. Chigarev, D. Yu. Paraschuk, X. Y. Pan, and V. E. Gusev, Phys. Rev. B **61**, 15837 (2000).
¹⁹D. M. Todorovic, P. M. Nikolic, A. I. Bojicic, and K. T. Radulovic, Phys. Rev. B **55**, 15631 (1997).
²⁰D. M. Todorovic, P. M. Nikolic, and A. I. Bojicic, J. Appl. Phys. **85**, 7716 (1999).
²¹D. M. Todorovic, Rev. Sci. Instrum. **74**, 582 (2003).
²²S. Dixon, C. Edwards, S. B. Palmer, and D. W. Schindel, J. Phys. D **29**, 1345 (1996).
²³A. Haug, Solid State Commun. **22**, 537 (1977).
²⁴A. Haug, Solid State Commun. **25**, 477 (1978).
²⁵H. W. Lord and Y. A. Schulman, J. Mech. Phys. Solids **15**, 299 (1967).
²⁶D. Royer and E. Dieulesaint, *Proceedings of the 1986 IEEE Ultrasonics Symposium*, (IEEE, New York, 1986), 527.
²⁷A. Moreau, D. Lévesque, M. Lord, M. Dubois, J.-P. Monchalain, C. Padioleau, and J. F. Bussière, Ultrasonics **40**, 1047 (2002).
²⁸H. J. Maris, Phys. Rev. B **28**, 7033 (1983).
²⁹T. Pearcey, Philos. Mag. **37** (264), 311 (1946).
³⁰K. Y. Kim, K. C. Bretz, A. G. Every, and W. Sachse, J. Appl. Phys. **79**, 1857 (1996).
³¹S. Guilbaud and B. Audoin, J. Acoust. Soc. Am. **105**, 2226 (1999).